

In-situ observation of successive crystallisations and metastable intermediates in metal-organic framework formation

Hamish H.-M. Yeung,^{*,[a, b]} Yue Wu,^[c] Sebastian Henke,^[d, e] Anthony K. Cheetham,^[e] Dermot O'Hare^[c] and Richard I. Walton^{*,[f]}

Abstract: Understanding the driving forces controlling crystallisation has important consequences ranging from the design of new materials to commercialisation. This is particularly relevant for metal-organic frameworks (MOFs), where mild solvothermal synthesis often allows access to related phases from the same reagents. Using high energy, *in-situ* synchrotron X-ray powder diffraction we have monitored the sequential crystallisations of three lithium tartrate MOFs, extracting the fundamental kinetic parameters of each interconversion. In particular, a rapidly-formed hydrated phase, **1**, is transformed to a structurally-similar metastable anhydrous phase, **2a**, with an activation energy of 41(3) kJ·mol⁻¹. Crystallization of the thermodynamic product, **2b**, promotes dissolution of **2a** but with a higher activation energy, 210(80) kJ·mol⁻¹. We have quantified the complete reaction energy profile of competing solvothermal crystallisations for the first time, and demonstrated new experimental and analytical methodology for the *in-situ* study of phase behaviour in the wider field of crystalline materials in general.

The formation mechanisms of crystalline materials from solution have long presented a challenge to researchers, owing to the multiple length-scales involved in the crystallization process. Yet understanding the driving forces of crystallization can have several profound effects, for example in polymorph selection, yield, purity and defect control. In MOFs, the synthesis of new porous materials for gas storage,^[1–3] catalysis^[4,5] and separations,^[6,7] as well as denser systems that exploit the synergy between organic and inorganic components, such as extreme flexibility,^[8–11] multiferroic behaviour,^[12,13] ion

dynamics^[14,15] and electronic conductivity,^[16–18] depends on a delicate interplay between dissolution, monomer formation, aggregation and formation of a bulk crystal lattice. No single technique can probe all the length-scales involved and, furthermore, the difficulty in designing *in-situ* experiments in the solvothermal conditions typical for MOFs has meant that only recently have such studies been reported.^[19–30] Of all the bulk *in-situ* techniques used to study MOF formation to date, energy-dispersive diffraction of white X-ray light is perhaps the most developed, allowing quantitative information about both crystal nucleation and growth to be extracted from changes in the intensities of single diffraction peaks, providing their origin is established *via* other, *ex-situ* methods.^[24,25,27–29]

As important as crystallisation kinetics are the underlying thermodynamics, which ultimately define the stability of competing reaction products. In MOFs, although related phases commonly crystallise from similar reagent mixtures, very little is known about the thermodynamic factors controlling their formation.^[31–33] In an effort to understand the competing formation of different MOF phases, we and others recently reported structural analyses and first-principles calculations of 14 dense lithium tartrate MOFs with the formula Li_{2-x}H_x(C₆H₄O₆)(H₂O)_y.^[34,35] Such unprecedented phase diversity enabled us to hypothesize that structures such as Li₂(*meso*-C₆H₄O₆)(H₂O)_{0.5}, **1**, and Li₂(*meso*-C₆H₄O₆), **2a**, with *gauche* ligand conformations - the preferred conformation of *meso*-tartaric acid^[36] - might be kinetic products, whilst the thermodynamically most stable phase, Li₂(*meso*-C₆H₄O₆), **2b**, which is 7.59 kJ·mol⁻¹ lower in energy than **2a** but has a non-equilibrium *trans*- ligand conformation, should have a higher activation barrier to its formation (Fig. 1).^[37,38] However, no study to date has been able to link fundamental thermodynamics of MOF formation with quantitative kinetics; even relative energies of reactants with respect to products remain undetermined.

- [a] Dr. H. H.-M. Yeung
International Center for Materials Nanoarchitectonics (MANA)
National Institute for Materials Science
Namiki 1-1, Tsukuba, Ibaraki 305-0044, Japan.
E-mail: YEUNG.Hamishheiman@nims.go.jp
- [b] Dr. H. H.-M. Yeung
International Center for Young Scientists (ICYS)
National Institute for Materials Science
Sengen 1-2-1, Tsukuba, Ibaraki, 305-0047, Japan.
- [c] Dr. Y. Wu and Prof. Dr. D. O'Hare
Chemistry Research Laboratory
University of Oxford,
Mansfield Road, Oxford, OX1 3TA, UK.
- [d] Dr. S. Henke
Lehrstuhl für Anorganische Chemie II
Ruhr-Universität Bochum
NC 2, Universitätsstrasse 150, 44801 Bochum, Germany.
- [e] Dr. S. Henke and Prof. Dr. A. K. Cheetham
Department of Materials Science and Metallurgy
Cambridge University
27 Charles Babbage Road, Cambridge, CB3 0FS, UK.
- [f] Prof. Dr. R. I. Walton
Department of Chemistry
University of Warwick
Coventry, CV4 7AL, UK.
Email: R.I.Walton@warwick.ac.uk

Supporting information for this article is given via a link at the end of the document.

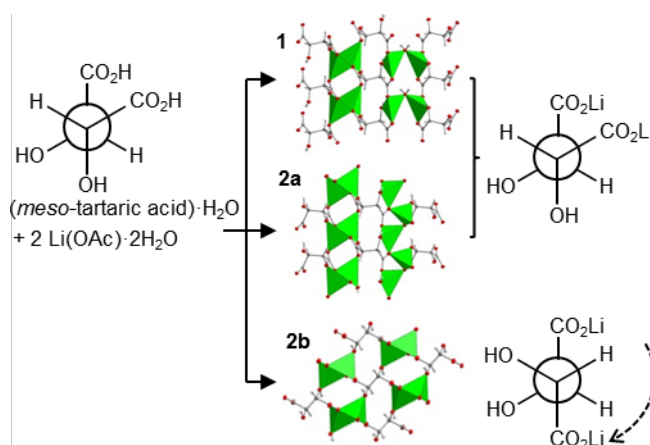


Figure 1. Possible products in the formation of lithium *meso*-tartrates, showing ligand conformations of each phase in Newman projection.

Table 1. Phase ID for formation of lithium *meso*-tartrates, showing reaction temperatures, rate constants and exponents extracted from kinetic modelling of *in-situ* X-ray diffraction data, plus final products and yields measured *ex-situ*.

Temp. / °C	First phase ^[a]					Second phase ^[b]					Final phase	
	ID	$k_N / 10^{-3} \cdot s^{-1}$	$k_G / 10^{-3} \cdot s^{-1}$	n_G	$k_D / 10^{-3} \cdot s^{-1}$	n_D	ID	$k_N / 10^{-3} \cdot s^{-1}$	$k_G / 10^{-3} \cdot s^{-1}$	n_G	ID	Yield / %
40.1(4)	1				0.93(7)	2.9(3)	2a	1.76(6)	0.574(7)	0.78(3)	2a	30
58(1)	1				11(3)	1.5(7)	2a	3.96(10)	2.43(13)	0.362(14)	2b	59
78(2)	2a	12.9(12)	3.25(7)	0.368(10)			-				2b	57
96.6(2)	2a		7.5(2)	0.291(7)			-				2a	39
104.4(3)	2a		12.3(7)	0.47(2)	7.25(13)	0.614(11)	2b	0.2262(3)	34.5(13)	0.577(14)	2b	66
111.0(4)	2a		8.9(5)	0.63(5)	10.4(3)	0.76(2)	2b	0.538(2)	210(40)	0.160(19)	2b	50
123.6(3)	2a		7.9(4)	0.73(4)	33.3(19)	0.50(2)	2b	0.3782(2)	430(140)	0.33(3)	2b	70

[a] Where the initial rise of the crystallisation curve occurred before data collection, nucleation parameters were not extracted. [b] At 78(2) °C and 96.6(2) °C, **2a** remained stable for the duration of the *in-situ* experiment.

In order to overcome the experimental challenges required to link thermodynamic insight with new kinetic parameters, we have performed *in-situ* diffraction using high energy, monochromatic X-rays to increase the detected range of *d*-spacings, enabling phase identification directly from the *in-situ* data. Reactions were performed in a large volume reactor, mimicking real laboratory conditions, between lithium acetate and *meso*-tartaric acid in water-ethanol at a series of temperatures between 40.1(4) and 123.6(3) °C (see S1 in the Supporting Information for details). Phase identification of the *in-situ* X-ray diffraction patterns reveal that formation of the thermodynamic product, **2b**, is preceded by two phases: first by the hydrated analogue, **1**, and subsequently by the metastable anhydrous polymorph, **2a** (see Fig. 2 and Figs. S1-7 in the SI). The progression of reaction products corresponds to increasing density and decreasing enthalpy of the structures in the order **1**→**2a**→**2b**, in agreement with Ostwald's rule of stages.^[39]

After development of a new crystallisation model to fit the changes in diffraction peak intensity (see following section), the rate constants and exponents could be extracted for most nucleation, growth and dissolution processes (Table 1). In general, the MOF formation reactions occur faster at higher temperatures, such that owing to the delay in data collection (150 – 180 s after the start of each reaction), the crystallisation of **1** is missed entirely and the initial rise of **2a** is missed above 96.6(2) °C. For these cases, we can simply make the qualitative observations that nucleation occurs faster than could be measured by our experiment, giving the nucleation rate constant, $k_N(\mathbf{1})$, a minimum value of $11 \times 10^{-3} \text{ s}^{-1}$ (conservatively assuming the time of peak nucleation, a_N , occurs midway between $t = 0$ and the start of data collection, 150-180 s).

Crystallisation of **2a** was observed at all temperatures, and the changes in integrated peak intensities were fitted using either the Avrami-Erofe'ev expression for crystal growth, $\alpha = G(t) = 1 - \exp(-(k_G \cdot t)^{n_G})$,^[40] or, where the initial rise was observed such that the effect of nucleation could be taken into account, the Gualtieri expression for crystal nucleation and growth, $\alpha = N(t) \cdot G(t) = 1/(1 + \exp((t-a_N)/b_N)) \cdot G(t)$,^[41] (see S2, Table S1 and Fig. S8 in the SI). Up to 104.4(3) °C, both $k_N(\mathbf{2a})$ and $k_G(\mathbf{2a})$ increase with temperature, as expected for a thermally activated process. The crystal growth exponent, $n_G(\mathbf{2a})$, is consistently less than unity, indicating that growth is surface reaction-limited, rather than diffusion limited.^[42] Unlike other MOF systems, for which n_G could be fixed at integer values suggestive of particle growth dimensionality,^[24,25,29,43] it appears as if particle morphology plays no rate-limiting role in the crystallization of the lithium *meso*-tartrates.

In the past, several equations, including power laws, have been used to model dissolution kinetics but with limited physical meaning ascribable to the fitted parameters.^[25,44] Given that both **2a** and **2b** form and interconvert with below-quantitative yields (Table 1), we may assume that lithium tartrate MOFs exist in dynamic equilibrium with dissolved precursors. It therefore seems reasonable to model the dissolution of **1** and **2a** as the time-reversed equivalent of crystal growth, i.e. the Avrami-Erofe'ev equation $D(t) = G(t_{0,D}-t) = 1 - \exp(-(k_D \cdot (t_{0,D}-t))^{n_D})$, where $t_{0,D}$ marks the end of the dissolution process, after which

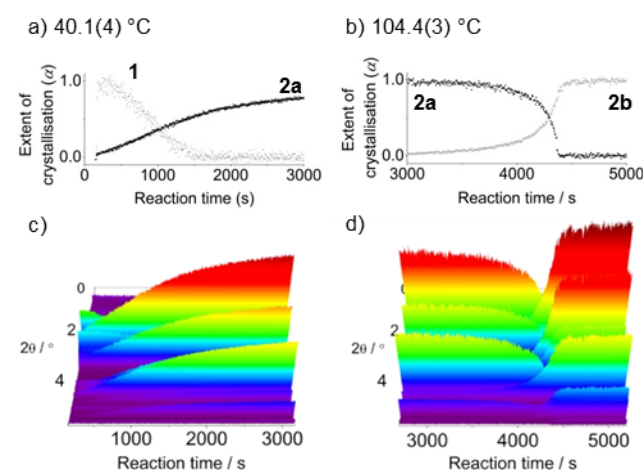


Figure 2. Solvothermal conversions between lithium tartrate MOFs: crystallisation curves (top) extracted from *in-situ* XRD data (bottom). a,c) hydrated phase **1** (crosses) to metastable phase **2a** (filled circles), and b,d) **2a** to the thermodynamic phase **2b** (open circles). $\lambda = 0.2326 \text{ \AA}$.

all subsequent growth of the new phase must come from diffraction-invisible species, i.e. monomeric species or dissolved nuclei. In this way, we can directly compare the rate constants and the exponents of crystallization and dissolution to provide meaningful insight into the reaction mechanisms of the different processes. Combining $D(t)$ with $G(t)$ in a single expression provides a good fit to the changes in integrated peak intensity over the course of the entire reaction for **1** and **2a** above 104.4(3) °C (see Table S2 and Figs. S9-10). Values of $n_D(\mathbf{1}) = 2.9(3)$ and $1.5(7)$ suggest that dissolution of **1** is multi-dimensional, with a heavily temperature-dependent rate constant k_D . In contrast, $n_D(\mathbf{2a})$ is, like $n_G(\mathbf{2a})$, consistently below unity, suggesting that the same reaction mechanism may indeed be responsible for the dissolution of **2a** as for its growth.

Above 104.4(3) °C, the crystallization of the thermodynamic product **2b** was observed. Owing to severe asymmetry in the sigmoidal crystallization curves - the long initial rise and short time to reach a plateau - neither Gualtieri nor Avrami-Erofe'ev crystallization models described the growth of **2b** adequately. Instead, we propose to split the two functions contained in the Gualtieri model into distinct sections separated by a refinable variable, $t_{0,G}$, which gives an estimate of the cross-over between the nucleation-related regime, which should be dependent on the dissolution of **2a**, and the growth-related regime, which should be independent: for $t < t_{0,G}$, $\alpha = N(t) = 1/(1 + \exp((t-a_N)/b_N))$, and for $t \geq t_{0,G}$, $\alpha = G(t) = 1 - \exp(-(k_G \cdot (t_{0,G} - t)^{n_G}))$. Despite the possibility of a discontinuity at $t = t_{0,G}$, the split Gualtieri model provides a much-improved fit to both the extended nucleation process and the crystal growth process (see Tables S3-4 and Figs. S11-12 in the ESI). Furthermore, since at each temperature $t_{0,G}(\mathbf{2b})$ lies close in time to $t_{0,D}(\mathbf{2a})$, we can be confident that the parameters $k_G(\mathbf{2b})$ and $n_G(\mathbf{2b})$ reliably describe the crystal growth of **2b**, independent of its nucleation kinetics and the dissolution of **2a**.

In general, there is no reason why simple nucleation-growth models such as those of Gualtieri and Avrami-Erofe'ev should fit well when we are dealing with successive transformations; the growth of the second phase must relate to the decay of the first, as well as any diffraction-invisible species already in solution. After formation of phase **2a** the concentration of reactant is lower than the initial concentration, and so the initial rise of **2b** takes longer compared to **2a**. As **2b** forms, **2a** acts to maintain the amount of the reactant in solution by gradually redissolving. Only once **2a** has completely dissolved (i.e. $t > t_{0,D} \approx t_{0,G}$) does the crystallization curve of **2b** resemble conventional crystal growth, with the plateauing in the crystallization curve a result of decreasing reactant concentration as it is used up to form **2b**.

Whilst $k_G(\mathbf{2b})$ increases with temperature, $k_N(\mathbf{2b})$ increases to 104.4(3) °C then decreases at 123.6(3) °C. We believe this may be due to the increasing importance of entropy at high temperatures, which is known to stabilise low density, metastable polymorphs.^[37,45] This results in higher yields of **2a** and therefore a lower concentration of reagent remaining in solution, further inhibiting the nucleation of **2b**. Similarly, $k_G(\mathbf{2a})$ decreases slightly above 104.4(3) °C, a likely effect of lower reactant concentrations induced by the competing crystallization of **2b**. The fact that $k_G(\mathbf{2b})$ is always several orders of magnitude larger than $k_G(\mathbf{2a})$ is a reflection of the larger overall driving force to form the thermodynamic product from the starting materials.

Activation energies, E_A , were calculated via Arrhenius plots of each rate constant versus $1/T$ (Fig. S13, Table S5). $E_{A,N}(\mathbf{2a})$ and $E_{A,G}(\mathbf{2a})$ have similar values, 51(6) kJ·mol⁻¹ and 41(3) kJ·mol⁻¹, respectively, suggesting that the same rate-determining process might happen for both. We hypothesize that the ligand-metal interactions with the necessary conformations for crystallization of **2a** and **2b** are generated via reactions at the growing crystal surfaces, as suggested by the low values of $n_G(\mathbf{2a})$ and $n_G(\mathbf{2b})$. These E_A values are lower than those of prototypical MOFs, HKUST-1 ($E_{A,N} = 71.6$ kJ·mol⁻¹) and MOF-14 ($E_{A,N} = 113.9$ kJ·mol⁻¹),^[25] indicative of the lability of the Li coordination sphere compared to transition metals such as Zn and Cu which are commonly used in porous MOFs. In contrast, $E_{A,G}(\mathbf{2b})$ is around four times higher at 210(80) kJ·mol⁻¹, indicative of the unfavourable change in ligand conformation necessary for the formation of **2b**. For the dissolution of **2a**, $E_{A,D}(\mathbf{2a}) = 90(20)$ kJ·mol⁻¹. To our knowledge, this is the first time that activation energies for both crystal growth and dissolution of one phase have been obtained from a single experiment. Somewhat unusually, this enables us to calculate a thermodynamic quantity from kinetic parameters without the need for expensive computation or intensive calorimetry. Subtracting $E_{A,G}(\mathbf{2a})$ from $E_{A,D}(\mathbf{2a})$ gives the energy difference between solvated reactants and crystalline products, $\Delta E_{rel}(\text{reactants-2a}) = 50(20)$ kJ·mol⁻¹.

Knowledge of the activation energies allows us to formally quantify the relationship between formation kinetics and thermodynamic stability of the lithium *meso*-tartrates for the first time. The reaction energy profile (Fig. 3) illustrates the energetics of the conversion of solvated reagents - lithium acetate and tartaric acid - to the MOF phases **1**, **2a** and **2b**. Relative energies of each phase are shown by the horizontal lines. The heights of the curves correspond to activation energies of crystal growth, $E_{A,G}$, and dissolution, $E_{A,D}$, quantifying the energetics of the structural changes (ligand conformation, metal binding modes etc.)^[37] needed to form each phase. It can be seen that as thermodynamic stability increases, so does the activation energy for the formation reaction.

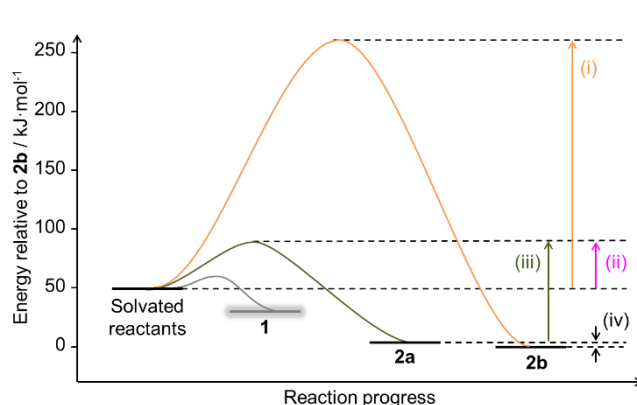


Figure 2. Quantitative energy profile for the formation of lithium *meso*-tartrate MOFs, showing experimentally determined activation energies i) $E_{A,G}(\mathbf{2b})$, ii) $E_{A,G}(\mathbf{2a})$, iii) $E_{A,D}(\mathbf{2a})$, and calculated thermodynamic stability iv) $\Delta E_{rel}(\mathbf{2a-2b})$. The energy profile of **1**, currently undetermined, is shown qualitatively for comparison.

In summary, we have been able to quantify the energetics of the crystallisation of a family of MOFs in terms of both kinetic and thermodynamic factors. The increased angular resolution obtained with high energy, monochromatic X-rays allows separation of the Bragg peaks of materials with low symmetry structures to an extent not possible with previously used energy-dispersive X-ray methods. Thus, using our setup we have been able to identify the temperature-dependent crystallisation and interconversion of three different lithium *meso*-tartrate phases, enabling rate constants and activation energies for nucleation, growth and dissolution to be derived by fitting two new kinetic models to the changes in peak intensity with time. The thermodynamically most stable phase, **2b**, forms *via* successive intermediates, **1** and **2a**, and requires a substantially larger activation energy to be overcome for its formation (210(80) kJ·mol⁻¹ vs. 41(3) kJ·mol⁻¹ for **2a**) owing to the unfavourable change in ligand conformation. This suggests that changes in ligand conformation might play a rate-limiting role in the formation of MOFs with flexible ligands, even when transition metals are used. In this system, the differences in crystallisation rates should enable isolation of metastable **2a**, which is just 7.59 kJ·mol⁻¹ higher in energy than **2b**, but not **1**, which is only fleetingly apparent at the lowest temperatures. In addition, our ability to extract *kinetic* activation energies for both crystallization and dissolution of **2a** from one experiment has enabled us to calculate the relative *thermodynamic* stability of the products with respect to the reactants. To the best of our knowledge, this work provides the most comprehensive understanding of the energetics of MOF formation to date, and provides improved experimental and analytical methodology for study of the synthesis and stability of the wider field of crystalline materials.

Acknowledgements

We thank Diamond Light Source for beamtime (beamline I12, reference EE9661) and Christina Reinhard for assistance, Andrew Jupe for providing FitChi and XYBruck programs and Tadashi Ozawa and Kiyotaka Iiyama for assistance with microscopy. HHMY acknowledges support from the World Premier International Research Center Initiative on Materials Nanoarchitectonics (WPI-MANA) from MEXT, Japan, and the Royal Society of Chemistry Journal Grants for International Authors for travel. SH acknowledges the Alexander von Humboldt Foundation for a Feodor Lynen Fellowship. YW acknowledges the EU Seventh Framework Programme grant agreement no. FP7-NMP4-LA-2012-280983, SHYMAN.

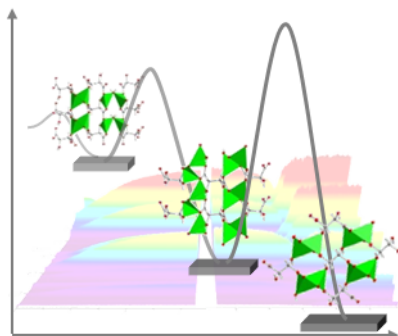
Keywords: crystallisation • metal-organic framework • kinetics • in-situ X-ray diffraction • intermediate

- [1] L. J. Murray, M. Dincă, J. R. Long, *Chem. Soc. Rev.* **2009**, *38*, 1294–1314.
- [2] J.-R. Li, R. J. Kuppler, H.-C. Zhou, *Chem. Soc. Rev.* **2009**, *38*, 1477–1504.
- [3] D. J. Tranchemontagne, K. S. Park, H. Furukawa, J. Eckert, C. B. Knobler, O. M. Yaghi, *J. Phys. Chem. C* **2012**, *116*, 13143–13151.
- [4] J. Lee, O. K. Farha, J. Roberts, K. A. Scheidt, S. T. Nguyen, J. T. Hupp, *Chem. Soc. Rev.* **2009**, *38*, 1450–1459.
- [5] L. Ma, C. Abney, W. Lin, *Chem. Soc. Rev.* **2009**, *38*, 1248–1256.
- [6] A. Comotti, S. Bracco, P. Sozzani, S. Horike, R. Matsuda, J. Chen, M. Takata, Y. Kubota, S. Kitagawa, *J. Am. Chem. Soc.* **2008**, *130*, 13664–72.
- [7] J.-R. Li, J. Sculley, H.-C. Zhou, *Chem. Rev.* **2012**, *112*, 869–932.
- [8] S. Henke, A. Schneemann, R. A. Fischer, *Adv. Funct. Mater.* **2013**, *23*, 5990–5996.
- [9] A. Schneemann, V. Bon, I. Schwedler, I. Senkovska, S. Kaskel, R. A. Fischer, *Chem. Soc. Rev.* **2014**, *43*, 6062–6096.
- [10] W. Cai, A. Katrusiak, *Nat. Commun.* **2014**, *5*, 4337.
- [11] M. T. Wharmby, S. Henke, T. D. Bennett, S. R. Bajpe, I. Schwedler, S. P. Thompson, F. Gozzo, P. Simoncic, C. Mellot-Draznieks, H. Tao, et al., *Angew. Chem., Int. Ed.* **2015**, *54*, 6447–6451.
- [12] P. Jain, V. Ramachandran, R. J. Clark, H. D. Zhou, B. H. Toby, N. S. Dalal, H. W. Kroto, A. K. Cheetham, *J. Am. Chem. Soc.* **2009**, *131*, 13625–7.
- [13] D.-W. Fu, W. Zhang, H.-L. Cai, Y. Zhang, J.-Z. Ge, R.-G. Xiong, S. D. Huang, T. Nakamura, *Angew. Chem., Int. Ed.* **2011**, *50*, 11947–51.
- [14] S. Horike, D. Umeyama, S. Kitagawa, *Acc. Chem. Res.* **2013**, *46*, 2376–2384.
- [15] S. Tominaka, S. Henke, A. K. Cheetham, *CrystEngComm* **2013**, *15*, 9400–9407.
- [16] A. A. Talin, A. Centrone, A. C. Ford, M. E. Foster, V. Stavila, P. Haney, R. A. Kinney, V. Szalai, F. El Gabaly, H. P. Yoon, et al., *Science* **2014**, *343*, 66–9.
- [17] D. Sheberla, L. Sun, M. A. Blood-Forsythe, S. Er, C. R. Wade, C. K. Brozek, A. Aspuru-Guzik, M. Dincă, *J. Am. Chem. Soc.* **2014**, *136*, 8859–8862.
- [18] S. Tominaka, H. Hamoudi, T. Suga, T. D. Bennett, A. B. Cairns, A. K. Cheetham, *Chem. Sci.* **2015**, *6*, 1465–1473.
- [19] S. Surblé, F. Millange, C. Serre, G. Férey, R. I. Walton, *Chem. Commun. (Cambridge, United Kingdom)* **2006**, 1518–1520.
- [20] S. Hermes, T. Witte, T. Hikov, D. Zacher, S. Bahnmüller, G. Langstein, K. Huber, R. A. Fischer, *J. Am. Chem. Soc.* **2007**, *129*, 5324–5325.
- [21] M. Shöäe, J. R. Agger, M. W. Anderson, M. P. Atfield, *CrystEngComm* **2008**, *10*, 646.
- [22] D. Zacher, J. Liu, K. Huber, R. A. Fischer, *Chem. Commun. (Cambridge, United Kingdom)* **2009**, *3*, 1031–1033.
- [23] J. Cravillon, S. Münzer, S. J. Lohmeier, A. Feldhoff, K. Huber, M. Wiebcke, *Chem. Mater.* **2009**, *21*, 1410–1412.
- [24] F. Millange, M. I. Medina, N. Guillo, G. Férey, K. M. Golden, R. I. Walton, *Angew. Chem., Int. Ed.* **2010**, *49*, 763–6.
- [25] F. Millange, R. El Osta, M. E. Medina, R. I. Walton, *CrystEngComm* **2011**, *13*, 103.
- [26] J. Cravillon, R. Nayuk, S. Springer, A. Feldhoff, K. Huber, M. Wiebcke, *Chem. Mater.* **2011**, *23*, 2130–2141.
- [27] T. Ahnfeldt, N. Stock, *CrystEngComm* **2012**, *14*, 505.
- [28] H. Reinsch, N. Stock, *CrystEngComm* **2012**, *15*, 544–550.
- [29] R. El Osta, M. Feyand, N. Stock, F. Millange, R. I. Walton, *Powder Diff.* **2013**, *28*, S256–S275.
- [30] M. Goesten, E. Stavitski, E. A. Pidko, C. Gücüyener, B. Boshuizen, S. N. Ehrlich, E. J. M. Hensen, F. Kapteijn, J. Gascon, *Chem. - Eur. J.* **2013**, *19*, 7809–7816.
- [31] L. N. Appelhans, M. Kosa, A. V Radha, P. Simoncic, A. Navrotsky, M. Parrinello, A. K. Cheetham, *J. Am. Chem. Soc.* **2009**, *131*, 15375–86.
- [32] R. Galvelis, B. Slater, A. K. Cheetham, C. Mellot-Draznieks, *CrystEngComm* **2012**, *14*, 374.
- [33] J. T. Hughes, T. D. Bennett, A. K. Cheetham, A. Navrotsky, *J. Am. Chem. Soc.* **2013**, *135*, 598–601.
- [34] H. H.-M. Yeung, M. Kosa, M. Parrinello, P. M. Forster, A. K. Cheetham, *Cryst. Growth Des.* **2011**, *11*, 221–230.
- [35] H. H.-M. Yeung, M. Kosa, M. Parrinello, A. K. Cheetham, *Cryst. Growth Des.* **2013**, *13*, 3705–3715.
- [36] A. Janiak, U. Rychlewska, M. Kwit, U. Stępień, K. Gawrońska, J. Gawroński, *ChemPhysChem* **2012**, *13*, 1500–6.
- [37] H. H.-M. Yeung, A. K. Cheetham, *Dalton Trans.* **2014**, *43*, 95–102.
- [38] For Cross-Referencing, the Phase Numbers Used in This Paper, *1, 2a and 2b, Correspond to Phases 11, 7, and 6, Respectively in Ref. [36]., n.d.*
- [39] W. Ostwald, *Zeitschrift für Phys. Chemie* **1897**, *22*, 289.
- [40] R. I. Walton, D. O'Hare, *J. Phys. Chem. B* **2001**, *105*, 91–96.
- [41] A. F. Gualtieri, *Phys. Chem. Miner.* **2001**, *28*, 719–728.
- [42] R. Viswanatha, D. D. Sarma, *Growth of Nanocrystals in Solution*, Wiley-VCH, **2007**.
- [43] R. El Osta, M. Frigoli, J. Marrot, M. E. Medina, R. I. Walton, F. Millange, *Cryst. Growth Des.* **2012**, *12*, 1531–1537.
- [44] P. J. Skrdla, *J. Pharm. Biomed. Anal.* **2007**, *45*, 251–256.
- [45] G. Kieslich, S. Kumagai, K. T. Butler, T. Okamura, C. H. Hendon, S. Sun, M. Yamashita, A. Walsh, T. Cheetham, *Chem. Commun.* **2015**, DOI 10.1039/C5CC06190C.

Entry for the Table of Contents

COMMUNICATION

Changing Phases: The relative stabilities and activation energies for the solvothermal formation of dense lithium *meso*-tartrate MOFs have been mapped out using high-energy *in-situ* X-ray powder diffraction. The thermodynamic product containing a non-equilibrium ligand conformation is accessed *via* the successive crystallisation and dissolution of two metastable intermediate phases.



Hamish H.-M. Yeung,* Yue Wu,
Sebastian Henke, Anthony K.
Cheetham, Dermot O'Hare & Richard
I. Walton*

XXXX – XXXX

**In-situ observation of successive
crystallisations and metastable
intermediates in metal-organic
framework formation**